Current Biology, Volume *24*

Supplemental Information

Local Control of Intestinal Stem Cell Homeostasis by Enteroendocrine Cells in the Adult *Drosophila* Midgut

Alessandro Scopelliti, Julia B. Cordero, Fengqiu Diao, Karen Strathdee, Benjamin H. White, Owen J. Sansom, and Marcos Vidal

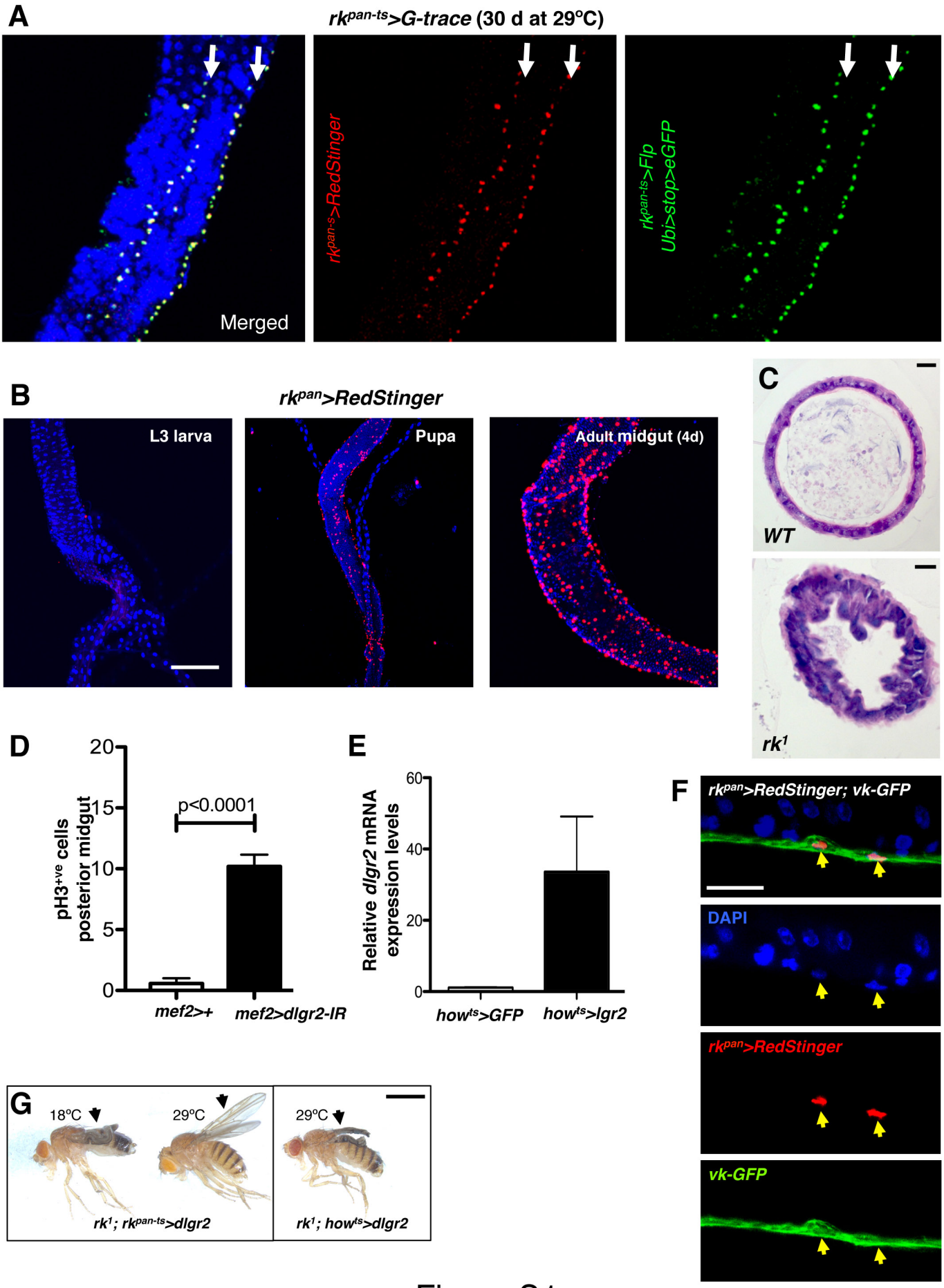
A
rkpan-ts>G-trace (30 d at 29ºC)
Merged
rkpan-s>RedStinger
rkpan-ts>Flp
Ubi>stop>eGFP
B
rkpan>RedStinger
L3 larva
Pupa
Adult midgut (4d)
C
WT
rk1
D
pH3+ve cells
posterior midgut
p<0.0001
mef2>+
mef2>dlgr2-IR
E
Relative dlgr2 mRNA
expression levels
how ts>GFP
how ts>lgr2
F
rkpan>RedStinger; vk-GFP
DAPI
rkpan>RedStinger
vk-GFP
G
18ºC
29ºC
29ºC
rk1; rkpan-ts>dlgr2
rk1; how ts>dlgr2

Figure S1

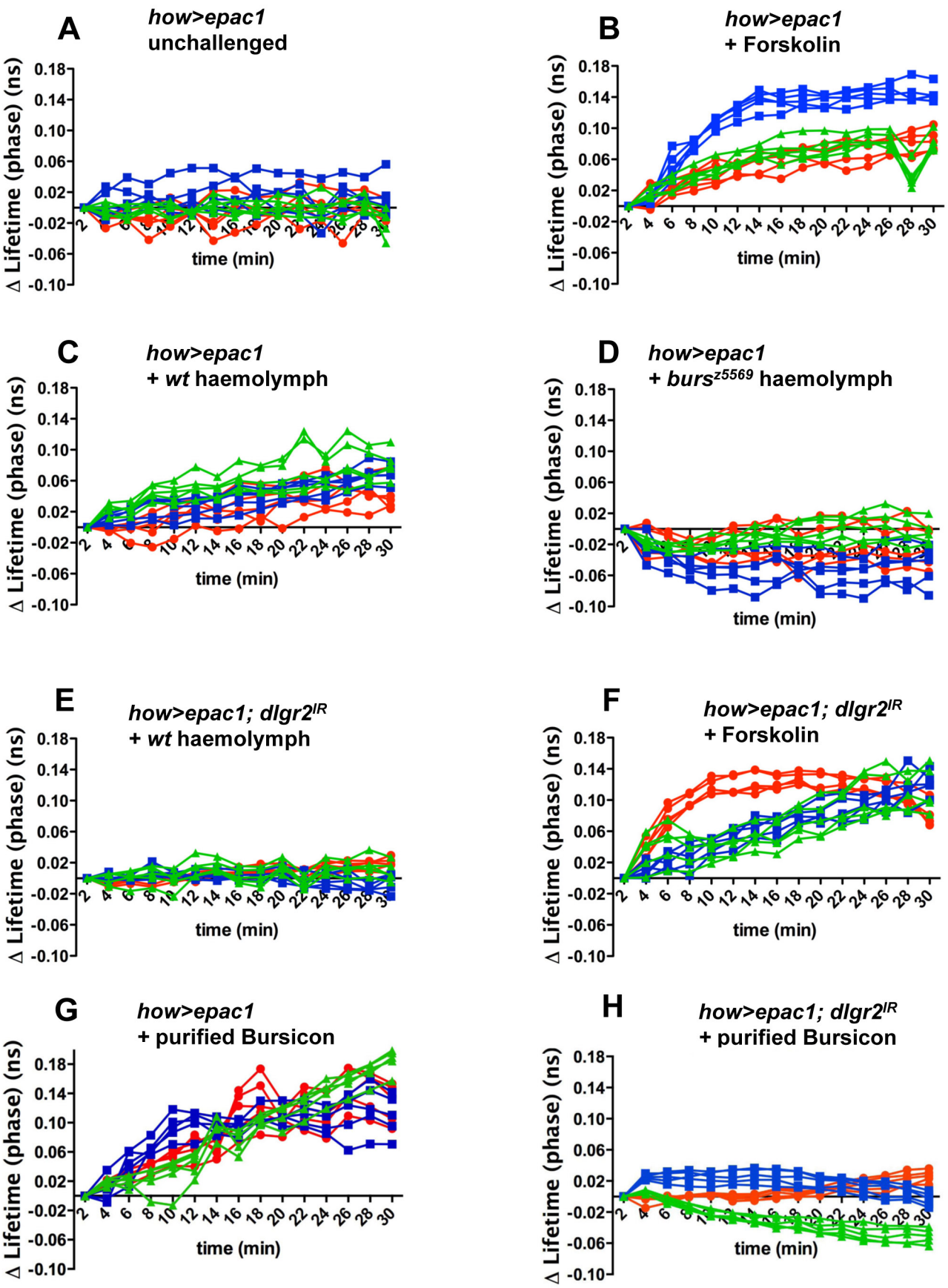
A
how>epac1
unchallenged
B
how>epac1
+ Forskolin
C
how>epac1
+ wt haemolymph
D
how>epac1
+ burs z5569 haemolymph
E
how>epac1; dlgr2 IR
+ wt haemolymph
F
how>epac1; dlgr2 IR
+ Forskolin
G
how>epac1
+ purified Bursicon
H
how>epac1; dlgr2 IR
+ purified Bursicon
Δ Lifetime (phase) (ns)
time (min)

Figure S2

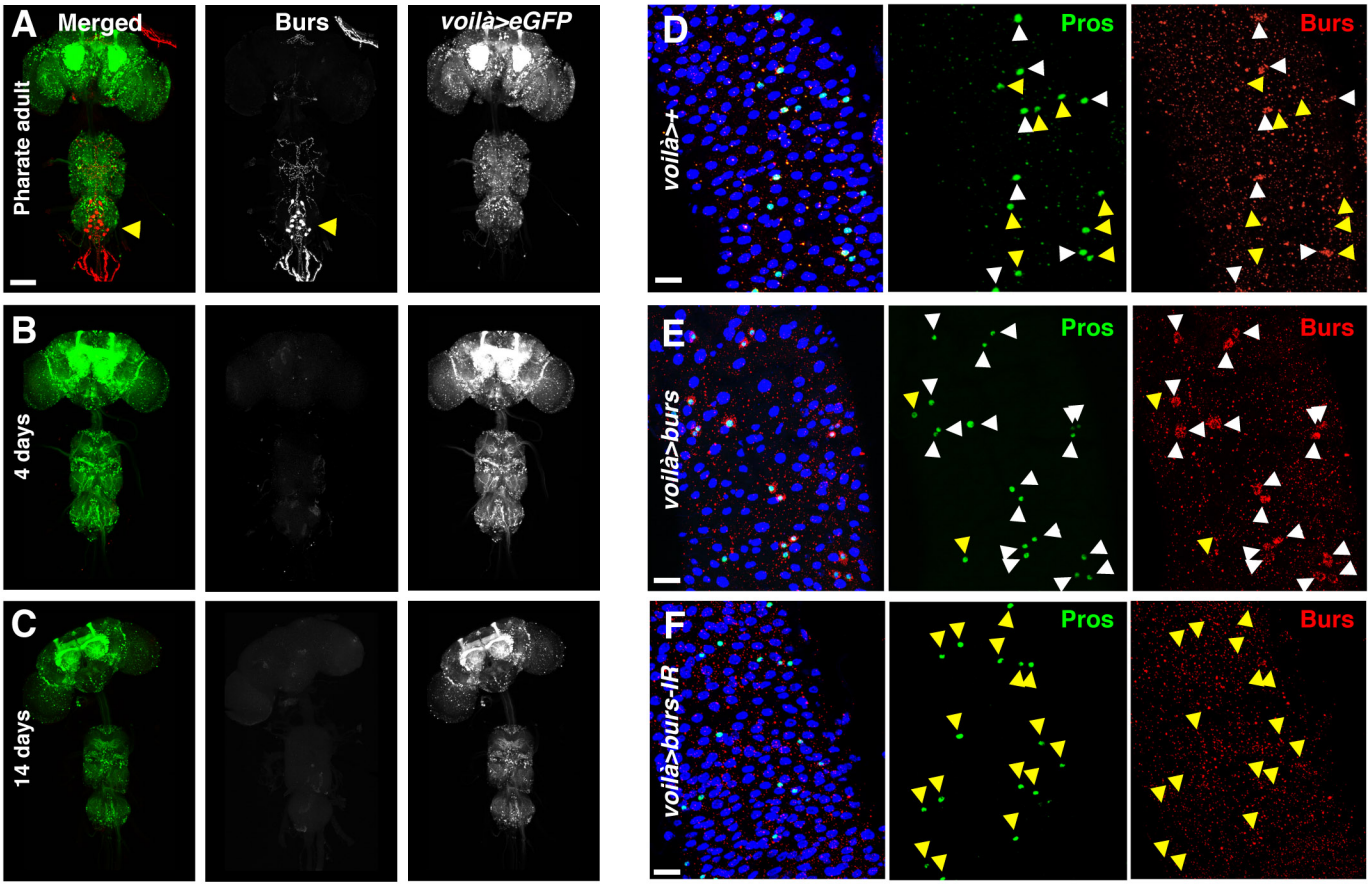
A
Merged
Burs
voilà>eGFP
Pharate adult
B
4 days
C
14 days
D
voilà>+
Pros
Burs
E
voilà>burs
Pros
Burs
F
voilà>burs-IR
Pros
Burs

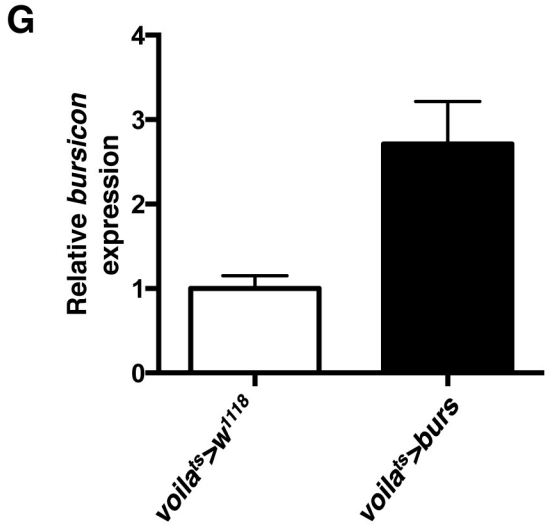
G
Relative bursicon expression
0
1
2
3
4
voilà^{ts}>w^{1118}
voilà^{ts}>burs

Figure S3

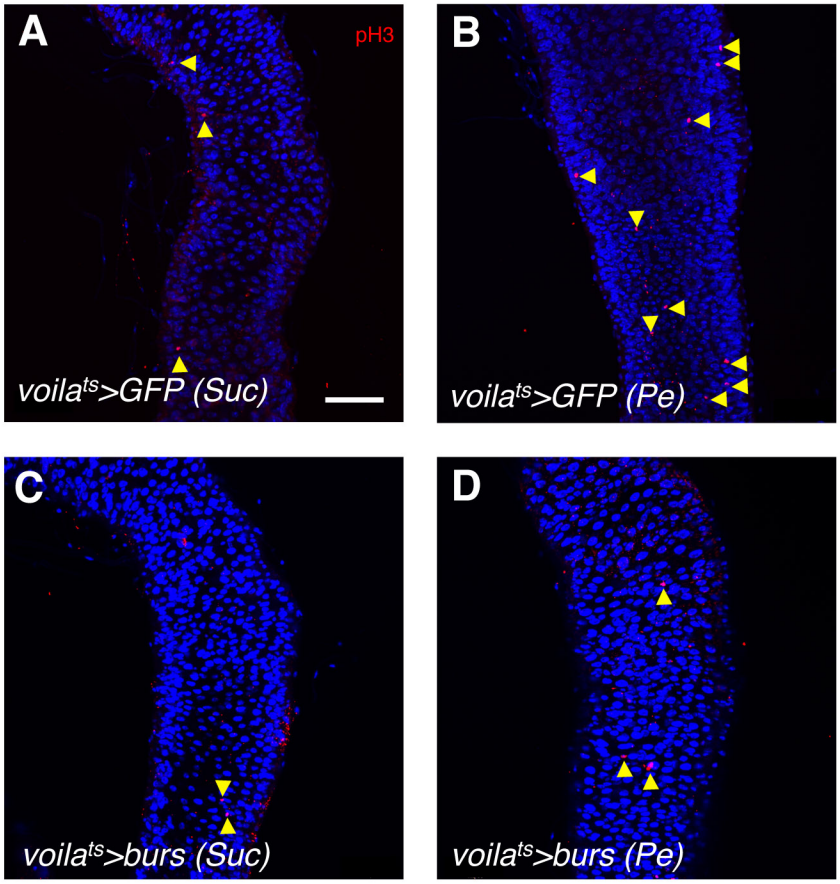
A
pH3
voilaᵗˢ>GFP (Suc)
B
voilaᵗˢ>GFP (Pe)
C
voilaᵗˢ>burs (Suc)
D
voilaᵗˢ>burs (Pe)

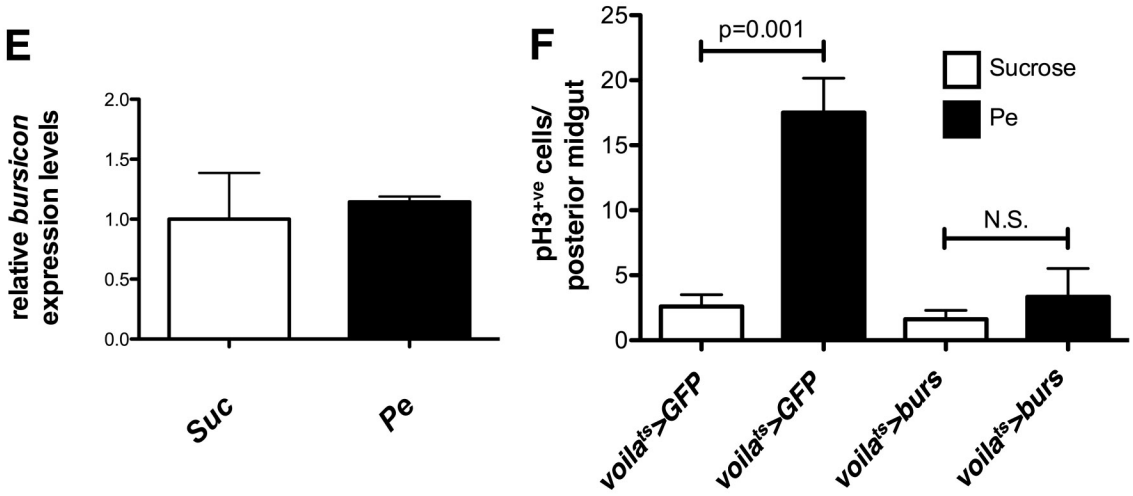
E
relative bursicon expression levels
2.0
1.5
1.0
0.5
0.0
Suc
Pe
F
pH3+ve cells/ posterior midgut
25
20
15
10
5
0
p=0.001
N.S.
Sucrose
Pe
voilaᵗˢ>GFP
voilaᵗˢ>GFP
voilaᵗˢ>burs
voilaᵗˢ>burs

Figure S4

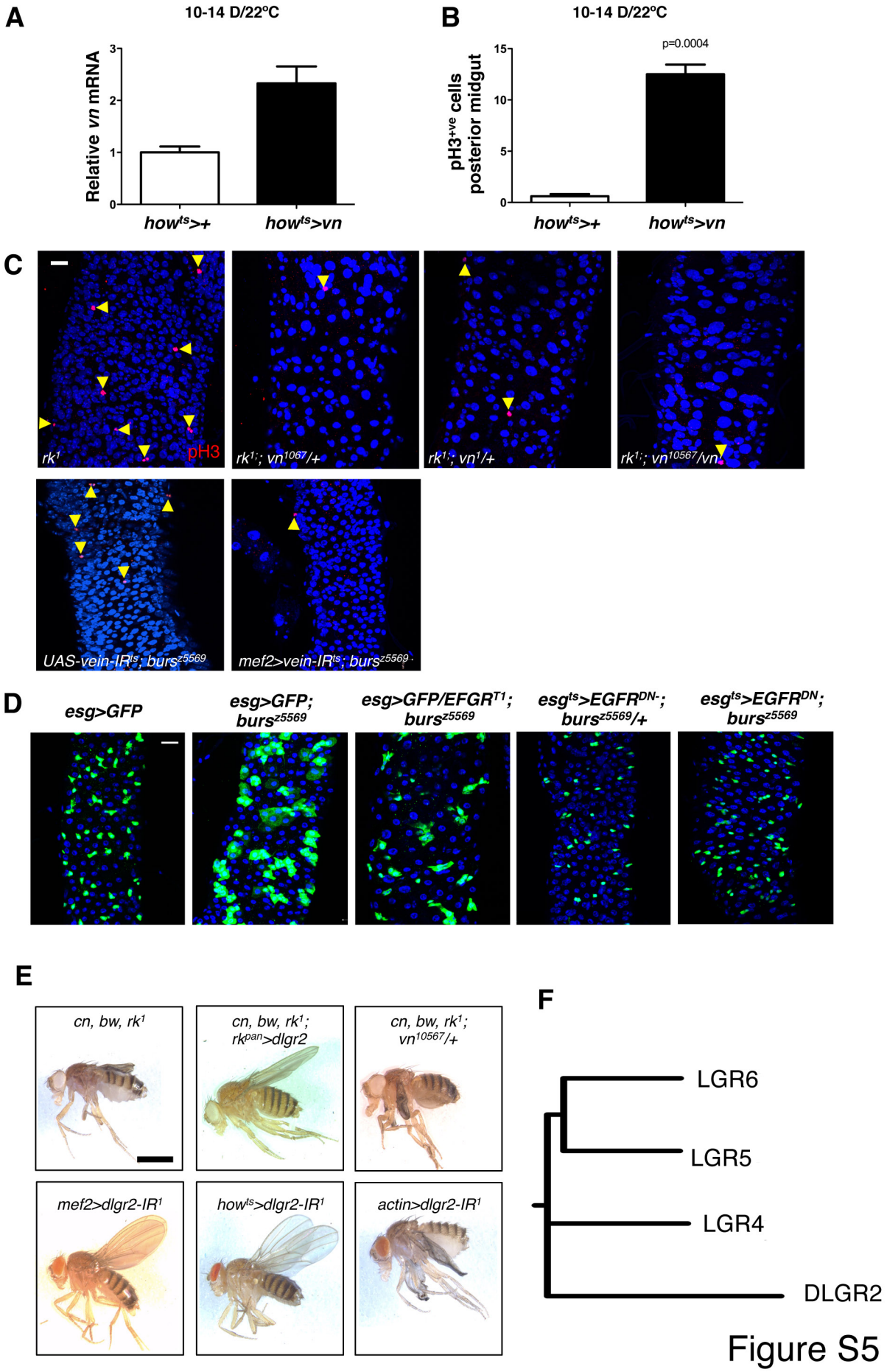
A
10-14 D/22ºC
Relative vn mRNA
how^ts>+
how^ts>vn
B
10-14 D/22ºC
p=0.0004
pH3+ve cells posterior midgut
how^ts>+
how^ts>vn
C
rk1
pH3
rk1; vn1067/+
rk1; vn1/+
rk1; vn10567/vn1
UAS-vein-IRts; burszz5569
mef2>vein-IRts; burszz5569
D
esg>GFP
esg>GFP; burszz5569
esg>GFP/EFGRT1; burszz5569
esgts>EGFRDN-; burszz5569/+
esgts>EGFRDN; burszz5569
E
cn, bw, rk1
cn, bw, rk1; rkpan>dlgr2
cn, bw, rk1; vn10567/+
mef2>dlgr2-IR1
hots>dlgr2-IR1
actin>dlgr2-IR1
F
LGR6
LGR5
LGR4
DLGR2

Figure S5

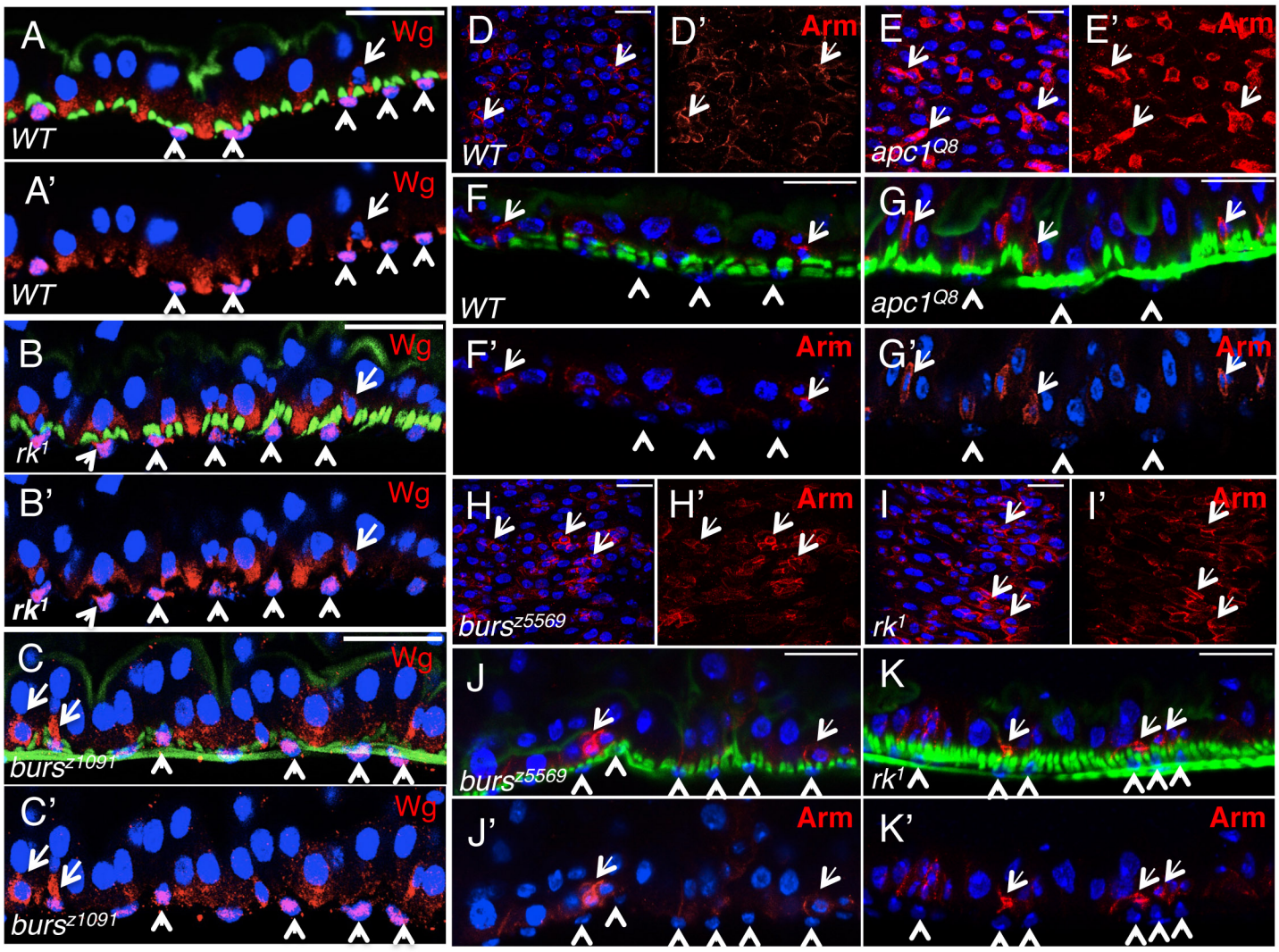
A
Wg
WT
A'
Wg
WT
B
Wg
rk1
B'
Wg
rk1
C
Wg
burs z1091
C'
Wg
burs z1091
D
WT
D'
Arm
E
apc1Q8
E'
Arm
F
WT
G
apc1Q8
F'
Arm
G'
Arm
H
burs z5569
H'
Arm
I
rk1
I'
Arm
J
burs z5569
K
rk1
J'
Arm
K'
Arm

Figure S6

***rpl32* f**	AGGCCCAAGATCGTGAAGAA
***rpl32* r**	TGTTGCACCAGGAACTTCTTGAA
***upd* f**	CCACGTAAGTTTGCATGTTG
***upd* r**	CTAAACAGTAGCCAGGACTC
***burs* f**	CATCCATGTGCTCCAGTATCC
***burs* r**	GGCTTCACTTTGGGACAGAA
***delta* f**	GGATCGGTGTTGAGTTGCTT
***delta* r**	TGTCTCATGTACGGCGGATA
***wg* f**	CCAACCCCACGAAGTACAGA
***wg* r**	CATGGATGGGGTGGTTTAAG
***dlgr2* f**	CAAACGCCAAGACTGAAGAG
***dlgr2* r**	GCTCGATAGATCTAACAGCCT
***vein* f**	GTGAAGTTGCCTGGATTCGT
***vein* r**	CTACAGGGAGCGACTGATGC

Supplementary Table 1: Sequences of the RT-qPCR primers used in this study.

Supplemental Information

Supplemental Figure legends

Figure S1. Related to Figures 1 and 2. *rk/dlgr2* is expressed in the visceral muscle (VM) to direct stem cell quiescence. (A) G-trace reporter driven by *rk^{pan}-gal4* in midguts after 30 days of linage tracing. In this G-trace system, nuclear RFP labels progenitor cells while the potential progeny could be identified by the presence of nuclear GFP and absence of RFP. Note that both reporters co-label visceral muscle cells only (arrows). DAPI (blue) labels all cell nuclei (left panel). **(B)** Posterior midguts from *rk^{pan}-gal4/UAS-RedStinger* animals dissected at the wandering L3 larval stage (left), 24h after puparium formation (middle) or at the adult stage (right). Scale bar: 100 µm. **(C)** Haematoxylin and Eosin staining of paraffin embedded sections from midguts of the indicated genotypes. Scale bar 20 µm. **(D)** Number of pH3^{+} cells per adult posterior midgut from animals with *rk/dlgr2* RNAi knockdown in the VM using the *mef2-gal4* driver. **(E)** RT-qPCR from 10-14 day old whole midguts of the indicated genotypes to assess relative *rk/dlgr2* transcript levels. **(F)** Confocal cross-section from a *rk^{pan}-gal4; UAS-RedStinger/vk-GFP* posterior midgut. *vk-GFP* (green) is a protein trap for Viking/Collagen IV and DAPI (blue) labels all cell nuclei. Arrows point to the two VM nuclei in the field, which were labeled with *rk^{pan}-gal4* (red) and are embedded within the extracellular matrix. Scale bar: 20 µm. **(G)** Stereo-micrographs of adult animals of the indicated genotypes and grown up at the indicated temperatures. Arrows point to wing phenotypes. Scale bar: 1mm.

Figure S2. Related to Figure 4. Bursicon increases VM cAMP via DLGR2. (A-H) Expansion of Figure 4B-D. The FRET/FLIM cAMP biosensor Epac1-camps was expressed in the VM via *how-gal4* and midguts imaged during the indicated time frame. Increases in the differential CFP/YFP lifetime fluorescence indicate increases in cAMP. The different treatments are indicated. Haemolymph was extracted from 0-1h old wild type or *burs* adults. In each panel, each curve is an individual measurement from each biological triplicate, highlighted by different colours.

Figure S3. Related to Figures 5 and 6. *Voilà-gal4* does not overlap with Burs^{+} CNS neurons and selectively controls Burs production in ee midgut cells. (A-C) Confocal projections from whole mount Central Nervous System (CNS) of *voilà>eGFP* animals. The age of the animals is indicated in days after adult eclosion. The tissues were stained with anti-Burs (red; left panels and grey; middle panels) and anti-GFP antibody (green; left panels and grey; right panels). The *voilà-gal4* insertion in the *prospero* locus was expressed in multiple neurons within the CNS. In contrast, Burs was expressed by a small subset of neurons within the abdominal and sub-esophageal ganglia of the pharate adult (arrowhead), which did not show detectable co-localization with *voilà>eGFP*. Bursicon expression was undetectable by immunostaining in the 4 and 14-day-old CNS. Scale bar 50 µm. **(D-F)** Co-immunostaining of Prospero (green; left and middle panels) and Burs (red; left and right panels) in midguts from 10-14 day old *voilà>+* (control;

D), *voilà>burs* **(E)** and *voilà>burs-IR* **(F)** animals. White arrows point to ee cells with detectable Burs expression and yellow arrows point to ee cells with undetectable Burs expression. Note that about 50% of the ee cells displayed Burs immunostaining in the control genotype. In contrast, most ee cells displayed strong Burs immunostaining in the over-expressing tissues, while Burs immunoreactivity was undetectable in ee cells upon RNAi knockdown. Scale bar: 20 µm. **(G)** RT-qPCR from 10-14 day old whole midguts of the indicated genotypes to assess relative *burs* transcript levels.

Figure S4. Related to Figure 6. Burs overexpression in ee cells prevents the proliferative response of ISCs to epithelial damage in the midgut. (A-D) Posterior midguts from control (*voilà>gfp*) and *burs* overexpressing (*voilà>*burs) animals fed with a sucrose (Suc) control solution **(A, C)** or with *Pseudomonas entomophila* (*Pe*) **(B, D)**. Tissues were stained with anti-pH3 (red) and counterstained with DAPI (blue). **(E)** RT-qPCR for levels of *burs* transcript relative to *rp49* in whole midguts of wild type control animals after Suc or *Pe* feeding. **(F)** Quantification of the number of $pH3^+$ cells in posterior midguts as in **A-D**. Note that Burs over-expression under *voilà-gal4* suppressed ISC proliferation in response to *Pe* infection. Scale bars: 20 µm.

Figure S5. Related to Figure 7. Vn and EGFR mediate ISC hyperproliferation in rk and *burs* midguts. (A) RT-qPCR from *how^{ts}>vn* whole midguts incubated at the indicated temperature shows 2-3 fold upregulation in relative *vn* transcript levels when compared to control (*how^{ts}>+*) midguts. **(B)** Quantification of the number of pH3^{+} cells per posterior midgut of animals with genotypes as in A. Mild *vein* overexpression in the VM phenocopies *rk* and *burs* mutant midguts. **(C, D)** Representative confocal projections from 10-14 days old posterior midguts of animal with the indicated genotypes as quantified in Figure 7F-H. Tissues were stained with anti-pH3 (C; red, arrowheads) or anti-GFP (D; green). DAPI (blue) stains all cell nuclei. Scale bars: 20 µm. **(E)** Stereo-micrographs from adult animals with the indicated genotypes. *rk* mutants displayed the characteristic wing inflation defects (upper left). DLGR2 expression via *rk^{pan}-gal4* background rescued the wing inflation phenotype of *rk* animals (upper middle). Removing one copy of *vn* in did not modify developmental defects in *rk* mutant animals (upper right). The expression of *dlgr2-IR* transgenes in muscle via *mef2-gal4* (lower left) or *how-gal4* (lower middle) did not affect wing inflation, while developmental defects were observed by ubiquitous expression of *dlgr2-IR* with *actin-gal4* (lower right). Scale bar: 1mm. Note that developmental defects in *rk/dlgr2* deficient animals are uncoupled from midgut phenotypes. **(F)** Phylogenetic relationship between mammalian LGR family members and DLGR2 created via Clustal W protein sequence alignments.

Figure S6. Related to Figure 7. Wg expression and signaling is not detectably altered in *rk* and *burs* adult midguts. (A-C) Confocal cross sections of 10-14 day-old posterior midguts from w^{1118} control **(A)**, *rk* **(B)** and *burs* **(C)** animals. Phalloidin (green) stains for F-actin to label the VM and epithelial brush border. Tissues were stained with anti-Wg (red) and counterstained with DAPI (blue). Top panels for each genotype show Phalloidin/Wg/DAPI overlay. Bottom panels show Wg/DAPI overlay. Arrows point to Wg-expressing cells within the midgut epithelium. Arrowheads point to Wg-expressing VM cells. Note that, consistent with the unchanged mRNA levels (Figure 7A), Wg protein levels in *rk* and *burs* midguts were comparable to that of control tissues. Scale bars: 10 µm. (**D-K')** Armadillo/β-catenin staining in *rk* and *burs* midguts**. D, D', E, E', H, H' I, I'**. Tangential confocal sections through the epithelium of posterior midguts from animals with the indicated genotypes, stained with anti-Armadillo (Arm; red). Nuclei were counterstained with DAPI (blue). Arrows point to ISCs, characterized by small size and enriched Arm staining (arrows). Note that *apc1* mutant midguts displayed significant accumulation of Arm within ISCs **E, E'**. In contrast, Arm staining in *burs* and *rk* midguts was not detectably different from that seen in control tissues, though the mutant midguts displayed increased numbers of ISCs per field consistent with our previous results (e.g.; Figure 2A). **F, F', G, G' J, J', K, K'.** Confocal cross sections from the posterior midguts shown in **D, D', E, E', H, H' I, I'.** Phalloidin (green) stains for F-actin to label the VM and epithelial brush border; DAPI (blue); anti-Arm (red). Top panels for each genotype show Phalloidin/Arm/DAPI overlay. Bottom panels show Arm/DAPI

overlay. Arrows point to Arm-expressing ISCs. Arrowheads point to VM cells. Note that Arm was undetectable in the VM from all the genetic backgrounds examined. Scale bars: 20 µm.

Movie S1: Bursicon increases cAMP in the midgut VM via DLGR2. Representative video files, used to quantify data displayed in Figure 4B. Purified Bursicon (150 nM) was added to control (*how>epac-camps,* top) or experimental (*how>epac-camps/dlgr2-IR,* bottom) midguts. Differential lifetime fluorescence (nanoseconds) is expressed in the indicated colour scale.

Movie S2. Related to Figure 1. Wild type tissue displayed a monolayered intestinal epithelium. : Rotating 3D view, obtained with Volocity software, from a wild type posterior midgut stained with DAPI (nuclei, blue) and Phalloidin (F-Actin, green). Note that the nuclei from the epithelial layer sit over the visceral muscle to form a monolayer.

Movie S3. Related to Figure 1: *rk* mutant tissue displayed a multilayered intestinal epithelium. Rotating 3D view, obtained with Volocity software, from a rk^{1} posterior midgut stained with DAPI (nuclei, blue) and Phalloidin (F-Actin, green). Note the multicellularity and multilayering within the intestinal epithelium.

Movie S4: Related to Figure 3: *burs* mutant tissue displayed a multilayered intestinal epithelium. Rotating 3D view, obtained with Volocity software, from a $burs^{5569}$ posterior midgut stained with DAPI (nuclei, blue) and Phalloidin (F-Actin, green). Note the multicellularity and multilayering within the intestinal epithelium.

Table S1. Primers used for quantitative RT-PCR.

Supplemental Experimental Procedures

Full genotypes from all Figures:

Figure 1

1. *w^{1118}; UAS-RedStinger; rk^{pan}-gal4*
2. *w^{1118}; UAS-RedStinger; rk^{pan}-gal4/vn^{10567}*
3. *UAS-dicer2; tub-$gal80^{ts}$; how-gal4*
4. *UAS-dicer2; tub-$gal80^{ts}$; how-gal4/UAS-dlgr2-$IR^{VDRC904}$*
5. *w^{1118};; mef2-gal4*
6. *w^{1118};; mef2-gal4/UAS-dlgr2-$IR^{VDRC904}$*
7. *w^{1118}*
8. *w^{1118}; rk^{1}/+*
9. *w^{1118}; rk^{1}*
10. *w^{1118}; rk^{1}/rk^{4}*

Figure 2

11. *UAS-dicer2; tub-$gal80^{ts}$; how-gal4*
12. *UAS-dicer2; tub-$gal80^{ts}$; how-gal4/UAS-dlgr2-$IR^{VDRC904}$*
13. *UAS-dicer2; tub-$gal80^{ts}$/UAS-dlgr2-$IR^{VDRC105360}$; how-gal4*
14. *UAS-dicer2; tub-$gal80^{ts}$/UAS-dlgr2-$IR^{VDRC105360}$; how-gal4/UAS-dlgr2*
15. *w^{1118}; rk^{1}; how-gal4*
16. *w^{1118}; rk^{1}; how-gal4/tub-$gal80^{ts}$, UAS-dlgr2*
17. *w^{1118}; rk^{1}; rk^{pan}-gal4*

18. *w^{1118}; rk^{1}; rk^{pan}-gal4/tub-gal80^{ts}, UAS-dlgr2*

19. *yw, hs-FLP, tub-gal4, UAS-GFP^{NLS}; FRT40A/tub-gal80, FRT40A*

20. *yw, hs-FLP, tub-gal4, UAS-GFP^{NLS}; rk^{1}, FRT40A/tub-gal80, FRT40A*

21. *yw, hs-FLP, tub-gal4, UAS-GFP^{NLS}; rk^{4}, FRT40A/tub-gal80, FRT40A*

Figure 3

22. *w^{1118}*

23. *w^{1118};; $burs^{1091}$/+*

24. *w^{1118};; $burs^{z5569}$/+*

25. *w^{1118};; $burs^{1091}$*

26. *w^{1118};; $burs^{z5569}$*

27. *w^{1118}; esg-gal4, UAS-GFP*

28. *w^{1118}; esg-gal4, UAS-GFP; $burs^{z5569}$*

Figure 4

29. *w^{1118}; UAS-CFP-Epac1-camps-YFP; how-gal4*

30. *w^{1118}; UAS-CFP-Epac1-camps-YFP/UAS-dlgr2-IR^{VDRC105360}; how-gal4*

31. *w^{1118}; tub-gal80^{ts}; rk^{pan}-gal4*

32. *w^{1118}, UAS-dnc; tub-gal80^{ts}; rk^{pan}-gal4/UAS-dnc*

33. *w^{1118}; UAS-PKA^{inh}/tub-gal80^{ts}; rk^{pan}-gal4/UAS-PKA^{inh}*

Figure 5

34. *w^{1118}; burs-gal4; UAS-eGFP*

35. *w^{1118}; burs-gal4*

36. *w^{1118}; burs-gal4/UAS-burs-IR*

37. *w^{1118}; burs-gal4/UAS-RedStinger*

Figure 6

38. *w^{1118}; esg-gal4, UAS-GFP*

39. *w^{1118}*

40. *w^{1118}; UAS-RedStinger; voilà-gal4*

41. *w^{1118}; tub-gal80^{ts}; voilà-gal4*

42. *UAS-dicer2; tub-gal80^{ts}/UAS-burs-IR; voilà-gal4*

43. *UAS-dicer2; tub-gal80^{ts}/UAS-burs-IR; voilà-gal4/UAS-burs*

44. *w^{1118}; tub-gal80^{ts}; voilà-gal4/UAS-burs*

Figure 7

45. *w^{1118}*

46. *w^{1118}; rk^{1}*

47. *w^{1118};; $burs^{z5569}$*

48. *w^{1118}; tub-gal80^{ts}; how-gal4/vn^{10567}*

49. *w^{1118}; tub-gal80^{ts}/UAS-dlgr2-IR^{VDRC105360}; how-gal4/vn^{10567}*

50. *UAS-dicer2; UAS-GFP/tub-gal80^{ts}; how-gal4*

51. *UAS-dicer2; UAS-vn-IR^{VDRC109437}/tub-gal80^{ts}; how-gal4*

52. *w^{1118}; tub-gal80^{ts}; rk^{pan}-gal4*

53. *w^{1118}, UAS-dnc; tub-gal80^{ts}; rk^{pan}-gal4/UAS-dnc*

54. *w^{1118}; UAS-PKA^{inh}/tub-gal80^{ts}; rk^{pan}-gal4/UAS-PKA^{inh}*

55. *w^{1118}; rk^{1}; vn^{10567}/+*

56. *w^{1118}; rk^{1}; vn^{1}/+*

57. *w^{1118}; rk^{1}; vn^{10567}/vn^{1}*

58. *UAS-dicer2; tub-gal80^{ts}; how-gal4*

59. *UAS-dicer2; UAS-vn-IR^{VDRC109437}/tub-gal80^{ts}; how-gal4*

60. *UAS-dicer2; tub-gal80^{ts}; how-gal4/UAS-dlgr2-IR^{VDRC904}*

61. *UAS-dicer2; UAS-vn-IR^{VDRC109437}/tub-gal80^{ts}; how-gal4/UAS-dlgr2-IR^{VDRC904}*

62. *w^{1118}; mef2-gal4; burs^{z5569}*

63. *w^{1118}; UAS-vn-IR^{VDRC109437}, tub-gal80^{ts}; burs^{z5569}*

64. *w^{1118}; UAS-vn-IR^{VDRC109437}, tub-gal80^{ts}/mef2-gal4; burs^{z5569}*

65. *w^{1118}; esg-gal4, UAS-GFP; burs^{z5569}*

66. *w^{1118}; esg-gal4, UAS-GFP/EGFR^{top1}; burs^{z5569}*

67. *w^{1118}; UAS-EGFR^{DN}, tub-gal80^{ts}; burs^{z5569}*

68. *w^{1118}; esg-gal4, UAS-GFP/UAS-EGFR^{DN}, tub-gal80^{ts}; burs^{z5569}*

Figure S1

69. *w^{1118};; UAS-RedStinger, tub-gal80^{ts}, UAS-FLP, ubi-FRT-stop-FRT-eGFP^{NLS}/rk^{pan}-gal4*

70. *w^{1118}; UAS-RedStinger; rk^{pan}-gal4*

71. *w^{1118}*

72. *w^{1118}; rk^{1}*

73. *w^{1118};; mef2-gal4*

74. *w^{1118};; mef2-gal4/UAS-dlgr2-IR^{VDRC904}*

75. *UAS-dicer2; UAS-GFP/tub-gal80^{ts}; how-gal4*

76. *UAS-dicer2; UAS-vn-IR^{VDRC109437}/tub-gal80^{ts}; how-gal4*

77. *w^{1118}; UAS-RedStinger/vk^{GFP}; rk^{pan}-gal4*

78. *w^{1118}; rk^{1}; rk^{pan}-gal4/tub-gal80^{ts}, UAS-dlgr2*

79. *w^{1118}; rk^{1}; how-gal4/tub-gal80^{ts}, UAS-dlgr2*

Figure S2

80. *w^{1118}; UAS-CFP-Epac1-camps-YFP; how-gal4*

81. *w^{1118}; UAS-CFP-Epac1-camps-YFP/UAS-dlgr2- $IR^{VDRC10536}$; how-gal4*

Figure S3

82. *w^{1118};; voilà-gal4/UAS-eGFP*

83. *w^{1118};; voilà-gal4*

84. *UAS-dicer2; UAS-burs-IR; voilà-gal4*

85. *w^{1118};; voilà-gal4/UAS-burs*

86. *w^{1118}; tub-gal80^{ts}; voilà-gal4*

87. *w^{1118}; tub-gal80^{ts}; voilà-gal4/UAS-burs*

88. **Figure S4***w^{1118}; tub-gal80^{ts}; voilà-gal4/UAS-eGFP*

89. *w^{1118}; tub-gal80^{ts}; voilà-gal4/UAS-burs*

Figure S5

90. *w^{1118}; tub-gal80^{ts}; how-gal4*

91. *w^{1118}; tub-gal80^{ts}; how-gal4/UAS-vn 1.2*

92. *w^{1118}; rk^{1}; vn^{10567}/+*

93. *w^{1118}; rk^{1}; vn^{1}/+*

94. *w^{1118}; rk^{1}; vn^{10567}/vn^{1}*

95. *UAS-vn-$IR^{VDRC109437}$, tub-gal80^{ts}; $burs^{z5569}$*

96. *w^{1118}; mef2-gal4/UAS-vn-$IR^{VDRC109437}$, tub-gal80^{ts}; $burs^{z5569}$*

97. *w^{1118}; esg-gal4, UAS-GFP*

98. *w^{1118}; esg-gal4, UAS-GFP; $burs^{z5569}$*

99. *w^{1118}; esg-gal4, UAS-GFP/$EGFR^{top1}$; $burs^{z5569}$*

100. *w^{1118}; esg-gal4, UAS-GFP/UAS-$EGFR^{DN}$, tub-gal80^{ts}; $burs^{z5569}$*

101. *w^{1118}; rk^{1}*

102. *w^{1118}; rk^{1}; rk^{pan}-gal4/UAS-dlgr2*

103. *w^{1118}; rk^{1}; vn^{10567}/+*

104. *w^{1118};; mef2-gal4/UAS-dlgr2-$IR^{VDRC904}$*

105. *w^{1118}; how-gal4/UAS-dlgr2-$IR^{VDRC904}$*

106. *w^{1118};; actin-gal4; UAS-dlgr2$IR^{VDRC904}$*

Figure S6

107. *w^{1118}*

108. *w^{1118}; rk^{1}*

109. *w^{1118};; $burs^{z1091}$*

110. *w^{1118};; $burs^{z5569}$*

111. *w^{1118};; FRT^{82B}, $Apc1^{Q8}$*

Intestinal epithelial damage/regeneration assay

Experimental flies were collected within 48h of eclosion at 18°C and moved to 29°C for 14 days on standard media. Flies were then transferred to either 5% sucrose (vehicle) or 10X overnight (*Pe*) culture on filter-paper discs (Whatman) for last day of the incubation period. Guts were then dissected and analyzed using immunofluorescence and confocal imaging.